AGU PUBLICATIONS

JGR

Journal of Geophysical Research: Earth Surface

RESEARCH ARTICLE
10.1002/2016JF004175

Key Points:
- Reduced-complexity flow modeling highlights arbitrary channel networks in topography data
- Modeling extends inundation-based mapping beyond observational constraints
- Maximum braiding index provides a basis for comparing multithread rivers

Correspondence to:
A. B. Limaye,
aslimaye@umn.edu

Citation:
Limaye, A. B. (2017). Extraction of multithread channel networks with a reduced-complexity flow model. *Journal of Geophysical Research: Earth Surface*, *122*. https://doi.org/10.1002/2016JF004175

Received 13 DEC 2016
Accepted 11 SEP 2017
Accepted article online 28 SEP 2017

Extraction of Multithread Channel Networks With a Reduced-Complexity Flow Model

Ajay B. Limaye[1]

[1]Department of Earth Sciences, St. Anthony Falls Laboratory, University of Minnesota, Minneapolis, MN, USA

Abstract Quantitative measures of channel network geometry inform diverse applications in hydrology, sediment transport, ecology, hazard assessment, and stratigraphic prediction. These uses require a clear, objectively defined channel network. Automated techniques for extracting channels from topography are well developed for convergent channel networks and identify flow paths based on land-surface gradients. These techniques—even when they allow multiple flow paths—do not consistently capture channel networks with frequent bifurcations (e.g., in rivers, deltas, and alluvial fans). This paper uses multithread rivers as a template to develop a new approach for channel extraction suitable for channel networks with divergences. Multithread channels are commonly mapped using observed inundation extent, and I generalize this approach using a depth-resolving, reduced-complexity flow model to map inundation patterns for fixed topography across an arbitrary range of discharge. A case study for the Platte River, Nebraska, reveals that (1) the number of bars exposed above the water surface, bar area, and the number of wetted channel threads (i.e., braiding index) peak at intermediate discharge; (2) the anisotropic scaling of bar dimensions occurs for a range of discharge; and (3) the maximum braiding index occurs at a corresponding reference discharge that provides an objective basis for comparing the planform geometry of multithread rivers. Mapping by flow depth overestimates braiding index by a factor of 2. The new approach extends channel network extraction from topography to the full spectrum of channel patterns, with the potential for comparing diverse channel patterns at scales from laboratory experiments to natural landscapes.

1. Introduction

Viewed from above, channels on planetary surfaces take on a variety of patterns. Many rivers on Earth transport water and sediment through a single channel, as in meandering rivers (e.g., Parker et al., 2011). But other channel networks include multiple channel threads that converge and diverge, including braided and anabranching rivers (Leopold & Wolman, 1957; Nanson & Knighton, 1996; Parker, 1976), or generally diverging channel branches, as in deltas. Several schemes have developed to classify river patterns based on planform geometry, morphodynamic processes, and the characteristics of bars, bank materials, and floodplains (Ashmore, 2013; Eaton, Millar, & Davidson, 2010; Kleinhans, 2010; Makaske, 2001; Nanson, 2013). Braided rivers have highly mobile sediment bars that are episodically inundated. In contrast, for anabranching rivers, bars are typically stabilized by vegetation (i.e., anastomosing), coarse sediment, or bedrock and consistently divide flow between channels (Nanson, 2013). Channel patterns commonly transform between headwaters and basin (Jerolmack & Mohrig, 2007), and over shorter scales. For example, the Platte River, Nebraska (Figure 1a), includes longitudinally extensive, multithread reaches with both braided (Figure 1b) and anabranching (Figure 1c) patterns alternating on scales of kilometers.

Across a range of landscapes, channel network geometry is a fundamental characteristic and a basis for reconstructing and predicting geomorphic change. Several methods have developed for efficient and automated channel extraction from topography data (e.g., Band, 1986; Sangireddy et al., 2016). These topography data have proliferated to global extent and meter-scale resolution (Farr et al., 2007; Passalacqua et al., 2015) and also represent the essential outputs of numerical landscape evolution models (Braun & Sambridge, 1997; Tucker & Hancock, 2010) and many physical experiments (e.g., Kim, Sheets, & Paola, 2010). To map channel networks, channel extraction methods commonly use surface gradients to predict zones of water accumulation from digital elevation models. This approach is effective in networks where channelized flow paths are largely convergent, hereafter referred to as type 1 channel networks. In contrast, a second class of channel networks include flow divergences. These features, hereafter referred to as type 2 channel networks, pose challenges to traditional channel extraction techniques for

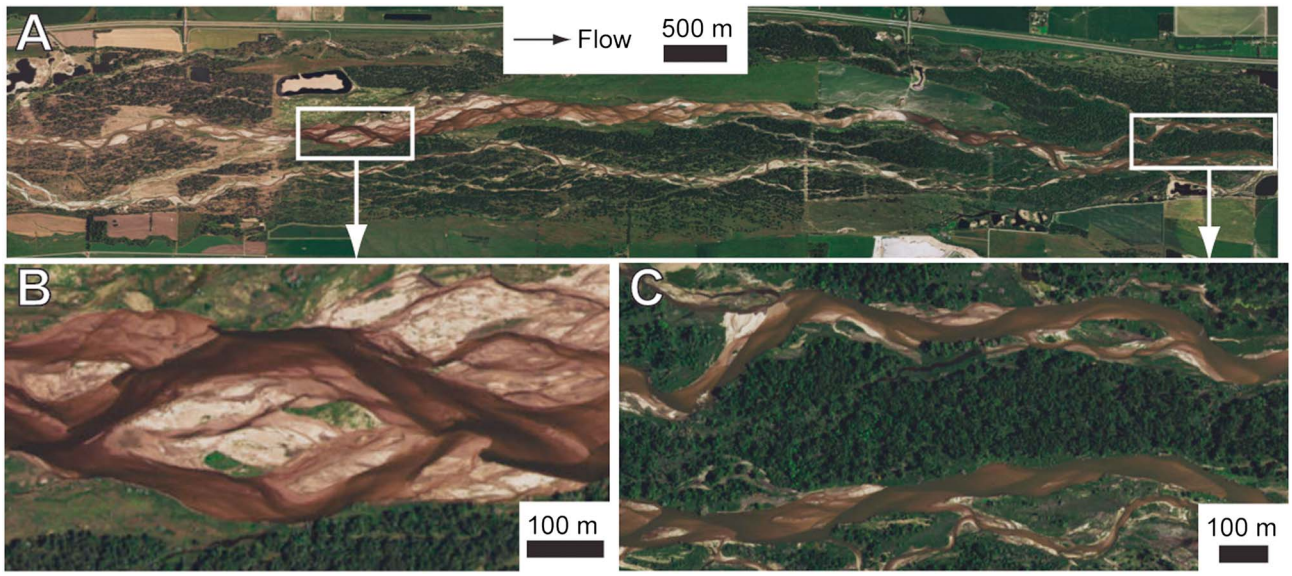

Figure 1. (a) The Platte River, Nebraska (40.67°N, 99.08°W). Channel patterns in this reach include (b) braiding and (c) anabranching, with bars stabilized by vegetation (anastomosed). Images: Google Earth.

topography data that are based on land surface gradients alone. This paper proposes an approach to mapping type 2 channel networks.

Multithread channels, which belong to type 2, are notable for their expression of channel and bar morphologies across a range of spatial scales and in diverse geologic settings. Braided channels form as a natural consequence of channel widening (Parker, 1976) and are commonly observed in areas of high sediment flux such as alluvial fans (Blair & McPherson, 1994) and in rivers in glacially influenced catchments (e.g., Reinfelds & Nanson, 1993). Channel networks with divergent flow paths are also observed on planetary surfaces. Examples include canyon systems and alluvial fans on Mars (Trevena & Picard, 1978; Williams & Malin, 2008); channels formed by lava on Earth, Mercury, Venus, and the Moon (Dietterich & Cashman, 2014; Komatsu & Baker, 1996; Leverington, 2011); and channels interpreted from backscatter images of Titan (Burr et al., 2013) and Earth's seafloor (Hesse et al., 2001).

The geometry of bars and channel networks affects a range of problems in planetary surface evolution. Planform geometry fundamentally distinguishes river types (e.g., Leopold & Wolman, 1957) and is the most accessible property of channels from remote sensing observations. Channel planform geometry records influences from discharge (Welber, Bertoldi, & Tubino, 2012), base level (Germanoski & Schumm, 1993), bank materials (Nanson, 2013), and vegetation (Bertoldi, Gurnell, & Drake, 2011; Tal & Paola, 2010). Channel network geometry is also a fundamental constraint for predicting hydraulics (Nicholas & Sambrook Smith, 1999); bulk fluxes of water (Lehner & Grill, 2013), sediment (Bertoldi, Ashmore, & Tubino, 2009; Kasprak et al., 2015), and contaminants (Coulthard & Macklin, 2003); and the propagation of floods and debris flows that pose significant hazards (Cavalli & Marchi, 2008). Channel and bar geometry shape habitat for fish and riparian species (Tockner et al., 2009; Van Der Nat et al., 2003) and inform models for groundwater and hydrocarbons in the subsurface (Anderson et al., 1999; Bridge & Lunt, 2006; Kelly, 2006).

Among type 2 channel networks, the spatial structure of multithread channel networks is complicated in comparison to type 1 channel networks for several reasons. First, channel pattern can evolve with increasing stage and include transitions between single-thread and multithread geometry (Mosley, 1982, 1983). Second, multithread rivers also show dynamic patterns of erosion and deposition that can alter channel pattern between successive floods (Lallias-Tacon, Liébault, & Piégay, 2014; Lane et al., 2010; Lane, Westaway, & Murray Hicks, 2003). In addition to these short-term dynamics, multithread channels evolve over scales of space and time that challenge direct observation. For example, for braided rivers the morphologically active portion may constitute less than half of the total channel belt (Ashmore, Bertoldi, & Gardner, 2011) and abandoned reaches may lie morphologically dormant for hundreds of years (Reinfelds & Nanson, 1993).

Third, bars and channels in multithread channels span a large range of scales (Kelly, 2006; Nykanen, Foufoula-Georgiou, & Sapozhnikov, 1998; Sapozhnikov & Foufoula-Georgiou, 1996, 1997).

For single-thread rivers, the bankfull discharge and associated channel geometry serve as useful properties for comparing rivers and for numerical modeling over geologic timescales. In contrast, the definition of a reference discharge that captures the planform geometry of multithread channels has proven problematic in cases due to the factors above (Rust, 1977). These qualities have complicated efforts to quantify the essential properties of multithread channel networks.

Despite these challenges, several workers have made key observations regarding the planform response of natural (Mosley, 1983) and experimental (Egozi & Ashmore, 2009) multithread channels to changes in discharge, the spatial structure of channel networks (Marra, Kleinhans, & Addink, 2014), and the scaling properties of bars (Kelly, 2006; Nykanen et al., 1998; Sapozhnikov et al., 1998; Sapozhnikov & Foufoula-Georgiou, 1996). For example, analyses of braided channels from laboratory experiments and natural cases for single discharges showed anisotropic scaling of bar dimensions, i.e., bar length and width increase at different rates as bar scale increases (Nykanen et al., 1998; Sapozhnikov & Foufoula-Georgiou, 1996).

The most common method for mapping the planform geometry of type 2 channel networks is to map inundation patterns. This straightforward approach has been applied to deltas (Edmonds et al., 2011) and has been used to document changes in wetted width and area, total channel sinuosity, the number of channel threads, and network properties for different discharges (e.g., Ashmore & Sauks, 2006; Marra et al., 2014; Mosley, 1983; Smith et al., 1996; Welber et al., 2012). Yet for both experimental and natural cases, mapping channel and bar structure using observed inundation has several limitations.

In laboratory experiments, flow is commonly dyed to facilitate automated channel mapping from images (Ashworth, Best, & Jones, 2007; Cazanacli, Paola, & Parker, 2002; Sapozhnikov & Foufoula-Georgiou, 1996; Wickert et al., 2013). This approach requires subjective image thresholds, and dye retention in sediments eventually blurs the distinction between bars and channels (Sapozhnikov & Foufoula-Georgiou, 1996). For both natural and experimental cases, submerged channel and bar structure may be obscured (Mosley, 1982).

For natural cases, the observational record of discharge variation is inherently limited in both range and resolution. Although this description applies to all channels, the limits of the observational record are most obvious for arid landscapes with highly intermittent flow (Blair & McPherson, 1994) and for abandoned channels with no historical record of inundation (e.g., Reinfelds & Nanson, 1993; Williams & Malin, 2008). Similarly, inundation cannot highlight channels in subaqueous environments. These factors motivate an alternative method to extract spatial structure for channels in natural and experimental settings independent of the observed, wetted extent of channels.

Channel topography, exposed at low flow, offers an alternative for objective geomorphic mapping. For example, local topographic statistics (e.g., slope, curvature, and roughness) have been used to map morphologic differences between alluvial fan lobes (Cavalli & Marchi, 2008; Frankel & Dolan, 2007; Staley, Wasklewicz, & Blaszczynski, 2006; Volker, Wasklewicz, & Ellis, 2007). Despite the evident topographic structure of bars, channels, and larger-scale lobes in multithread channel belts and fans, no existing methods objectively and rapidly identify these structures from topography alone.

This paper proposes to extend the existing, inundation-based approach to mapping type 2 channel networks by using a reduced-complexity flow model—not for morphodynamic modeling, but rather to analyze topography and to define bars and channels. Section 2 describes existing approaches for extracting type 1 channel networks using reduced-complexity flow modeling. Section 3 compares two flow modeling approaches for a type 2 channel network on the Platte River. These approaches include (1) a model driven by topographic slope alone and (2) a model that additionally accounts for the water surface. I also present a simple method for extracting type 2 channel networks based on the results of the latter flow modeling approach. Section 4 applies the mapping approach to defining bar and channel structure for the Platte River. Section 5 compares the results in section 4 to those from a complementary mapping approach that reverses the roles of discharge and flow depth in identifying channels. I discuss strengths and limitations of mapping by modeled inundation and recommendations for selecting representative bar and channel maps in section 6.

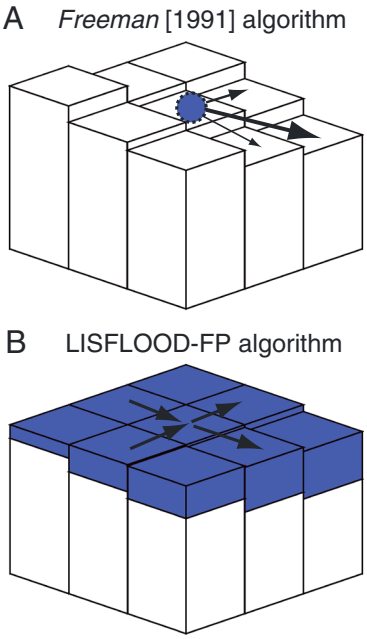

Figure 2. Schematics of reduced-complexity flow models applied to topographic grids. (a) The Freeman (1991) multiple flow path algorithm distributes a fictitious flow (blue sphere) from a cell to each of the downslope neighboring cells. (b) The LISFLOOD-FP algorithm (Bates et al., 2010) accounts for the water surface (blue) and routes flow through each cell along the rows and columns separately (arrows).

2. Background

2.1. Existing Approaches to Channel Extraction From Topography

The basic problem we face is to define a network of channels with bifurcations using a digital elevation model (DEM). In principle, flow paths may be calculated by solving the depth-averaged (Segura & Pitlick, 2015) or three-dimensional, Reynolds-averaged Navier-Stokes equations (Hardy, 2008; Williams et al., 2013). Indeed, several studies have successfully applied such models to flow and sediment transport for multithread rivers (Williams, Brasington, & Hicks, 2016). As a by-product, these model applications have generated inundated extents that could be used to extract network geometry. At present, however, there is no framework for using numerical models to extract channel networks from topography data in a way that (1) can be applied to type 2 channel networks in general, with minimal parameterization and for diverse planetary surface environments; (2) balances accuracy with computational complexity, to enable channel mapping at high spatial resolution and/or over large areas; and (3) systematically accounts for the effect of changing inundation on network geometry. As a starting point, we can consider approaches that have addressed the first two of these challenges for type 1 channel networks.

Type 1 channel networks are most commonly extracted from a DEM using either of two general approaches. In the first approach, the channel network is extracted using local topographic statistics, including relief, and for channels with widths near the DEM resolution, curvature (Fagherazzi et al., 1999; McKean et al., 2009; Pirotti & Tarolli, 2010). Neither measurement is designed to account for the role of flow paths in defining channel networks. In the second and more common approach, single-thread channels are identified as areas of water accumulation using a simplified flow model. Flow paths are approximated using surface gradients between adjacent cells in a DEM, which enables rapid computations over large grids. Drainage area is computed for each cell, and drainage area is used to identify the channel network directly (Band, 1986; Tarboton, 1997; Tarboton, Bras, & Rodriguez-Iturbe, 1991) or through a weighting procedure (Passalacqua et al., 2010). The calculation typically includes a sink-filling operation to prevent the flow trapping in local elevation minima (e.g., Garbrecht & Martz, 1997). Together, flow routing and sink-filling algorithms have been applied at catchment (Freeman, 1991; Shelef & Hilley, 2013) and orogen scales (Pelletier, 2004). A known limitation of the approach is that channel width is not resolved for channels wider than the grid spacing, and the flow paths often turn sharply within such channels due local slopes in the DEM (Passalacqua, Belmont, & Foufoula-Georgiou, 2012). Yet for extracting the skeleton of a type 1 channel network, the simplicity and computational efficiency of these models far outweigh the benefits of more complicated flow models.

Importantly, type 1 channel networks are typically composed of single-thread channels with generally convergent flow paths. These flow paths can be approximated by reduced-complexity flow models that use only surface slope (Shelef & Hilley, 2013). In contrast, some channels possess locally divergent flow paths in which the relationship between flow and topography is more complex. The form of such channels is not well captured in commonly used flow routing and channel extraction algorithms (Montgomery & Foufoula-Georgiou, 1993; Moore, O'Loughlin, & Burch, 1988). Bifurcations pose a significant challenge because they interrupt the monotonic increase in contributing area that forms the basis for extraction of convergent channel networks (Passalacqua et al., 2010; Sangireddy et al., 2016).

Reduced-complexity flow models differ in the number and orientation of driving topographic gradients and resulting flow directions (Figure 2). In one class of models, a fictitious flow is introduced to all cells in a DEM and routed downslope in a single flow direction determined by the direction of steepest descent (O'Callaghan & Mark, 1984; Shelef & Hilley, 2013; Tarboton, 1997). Alternatively, water can be distributed among multiple downslope directions (Band, 1986; Freeman, 1991; Holmgren, 1994; Quinn et al., 1991).

For example, in the Freeman (1991) model the flow fraction distributed from a center cell to a downslope cell i is

$$f_i = \frac{\max\left(0, S_i^p\right)}{\sum_{j=1}^{8} \max\left(0, S_j^p\right)} \quad (1)$$

where S_j represents the slope to each of the eight nearest neighbor cells and p is a dimensionless parameter commonly set to 1.1 (Freeman, 1991). Figure 2a shows a schematic of this algorithm wherein flow is distributed to all cells at lower elevations, with more flow apportioned across steeper downslope gradients. Section 3 tests the suitability of this approach for extracting channels with diverging flow paths using the Terraflow algorithm, which incorporates multiple flow paths (equation (1)) and sink filling, and is efficient for large grids (Arge et al., 2003).

Murray and Paola (1994) introduced a different class of reduced-complexity flow model specifically for braided rivers that permits flow over adverse slopes common in riverbed topography. Subsequent, related models (Thomas & Nicholas, 2002; Thomas, Nicholas, & Quine, 2007) assume a unidirectional water surface slope, and therefore cannot route flow in directions opposite the mean valley slope, nor across arbitrary spreading angles. Other two-dimensional hydrodynamic models, including LISFLOOD-FP (Bates, Horritt, & Fewtrell, 2010), are more geometrically flexible while still prioritizing computational efficiency.

Multiple flow path algorithms treat flow divergence more effectively than single path, steepest descent algorithms (Coulthard, Hicks, & Van De Wiel, 2007; Pelletier, 2004). This paper focuses on two particular multiple flow path algorithms: the Freeman (1991) algorithm based on topographic slope only and the LISFLOOD-FP algorithm that additionally accounts for water surface slope and therefore entails a greater computational cost. The next section describes the details of the latter model, which provides a basis sufficient to extract channel networks with arbitrary channel geometry.

2.2. The LISFLOOD-FP Flow Model

LISFLOOD-FP is integrated in the CAESAR-LISFLOOD landscape evolution model and uses an approximation of the shallow water equations to represent flow across a structured DEM (Bates et al., 2010; Coulthard et al., 2013). Water is transferred from a central grid cell to any of the four neighboring cells excluding diagonals (Figure 2b). The routing model is applied column-wise and then row-wise to simulate two-dimensional flow. A semi-implicit friction formulation is used for stability. The model is only strictly valid for subcritical and gradually varied flow, and therefore roughly approximates flow for cases that do not meet these conditions (Coulthard et al., 2013). Volumetric discharge between cells is calculated as

$$Q = \frac{q - gh_{\max}\Delta t \frac{\Delta(h+z)}{\Delta x}}{\left(1 + gh_{\max}\Delta t n^2 \left|q\right| / h_{\max}^{10/3}\right)} \Delta x \quad (2)$$

where q is the width-averaged water flux between cells, g is gravitational acceleration, h is flow depth, $h_{\max}$ is the maximum flow depth, Δt is the time step, z is elevation, Δx is the DEM grid spacing, and n is Manning's coefficient. In natural river corridors, roughness varies due to several channel and floodplain characteristics including topography, sediment grain size, and vegetation. In turn, roughness directly influences flow depth, and therefore inundation. In the spirit of existing channel extraction methods that rely on topography alone and without detailed hydraulic parameterization, this paper assumes uniform roughness ($n = 0.03$) characteristic of open channel flow (Chow, 1959). Table 1 summarizes the DEM characteristics and flow model parameters.

Table 1
DEM Characteristics and Flow Model Parameters for the Platte River Case Study

DEM properties		Flow model parameters					
Grid dimensions	Grid spacing (m)	Discharge range (m^3/s)	Manning's n	Number of discharge levels	Maximum difference between input and output discharge	Model run time (hours)	α
242 × 1078	10	10 to 1000	0.03	20	5%	3	0.7

Note. The dimensionless coefficient α scales the maximum time step for the flow model.

The change in water depth at a cell is calculated using conservation of water mass in the column (x) and row (y) directions

$$\frac{\Delta h^{i,j}}{\Delta t} = \frac{Q_x^{i-1,j} - Q_x^{i,j} + Q_y^{i,j-1} - Q_y^{i,j}}{\Delta x^2} \tag{3}$$

where i and j are the row and column coordinates, respectively, of cells in the DEM and Q_x and Q_y are the column-wise and row-wise volumetric discharges, respectively. The maximum time step (Δt_{max}) is set to meet the Courant-Friedrichs Lewy condition for shallow-water conditions

$$\Delta t_{max} = \alpha \frac{\Delta x}{\sqrt{gh}} \tag{4}$$

where α is a dimensionless coefficient, fixed here at 0.7.

To apply this flow model to landscapes, water is explicitly introduced as precipitation or from one or more point sources (Coulthard et al., 2013). Here water emanates from a source located upstream of the study reach; the implementation for the Platte River is discussed in section 3. Introducing flow from a localized source represents an important distinction from flow routing algorithms that use accumulation area as a proxy for discharge (e.g., Freeman, 1991), as for these algorithms the inclusion or exclusion of surrounding areas can influence drainage area (Shelef & Hilley, 2013). In contrast, the use of a localized flow source with the LISFLOOD-FP model ensures that contributing area does not influence the model results.

2.3. Morphometrics for Multithread Channels and Bars

After a channel network is extracted, a range of statistics can characterize its morphology. The statistics available depend in part on the network geometry. Whereas common channel planform statistics are relatively few and clearly defined for single-thread channels (Leopold & Wolman, 1960; Williams, 1986), the spatial statistics of multithread channels are numerous (Howard, Keetch, & Vincent, 1970) and their definitions still debated (Egozi & Ashmore, 2008). Planform geometry is not the only framework for interpreting multithread rivers; for example, Paola (1996) and Redolfi et al. (2016) propose to describe braided rivers using elevation distributions. Yet most quantitative measures of spatial structure for braided rivers relate to the planform geometry of bars and channels. Bar properties include the number and shape of bars, including area, length, and width (Kelly, 2006). Channel planform metrics include the bifurcation-confluence distance (Hundey & Ashmore, 2009) and network statistics (De Bartolo et al., 2006; Gleyzer et al., 2004; Marra et al., 2014; Passalacqua, 2016). Braided channel patterns are often quantified using the braiding index or intensity, which can be defined as the number of active channels or the summed sinuosity of all channel threads (Brice, 1964; Egozi & Ashmore, 2008; Howard et al., 1970).

The present analysis focuses on bar geometry and the number of channels. Bar measures include bar area (A_{bar}) and bar length (L_{bar}) and bar width (w_{bar}), measured as the semimajor and semiminor axes of a fitted ellipse, respectively. The braiding index (i.e., number of channels) is measured by counting the number of transitions from dry to wetted areas along a cross section of the braid plain oriented perpendicular to the mean downstream direction. To account for spatial variability in the number of channels measured in a cross section, I follow Egozi and Ashmore (2008) and average measurements for 10 cross sections spaced at approximately one half the width of the braid plain. In dimensionless form, bar metrics include the bar aspect ratio (i.e., L_{bar}/w_{bar}) and the total dimensionless bar area

$$\sum A^*_{bar} = \frac{\sum A_{bar}}{L_{bp} L_z} \tag{5}$$

where $\sum A_{bar}$ is the summed area of all bars and L_{bp} is the length of the braid plain.

2.4. Case Study: The Platte River

The Platte River serves as a trial location for the topographic analysis approach. The Platte River drains the Rocky Mountains in the western portion of the Mississippi River watershed and is a longstanding location for multithread river studies (Smith, 1971). The regional climate is semiarid, and under natural conditions snowmelt drives discharge peaks during spring and early summer (Fotherby, 2009; US Dept. Interior, 2006).

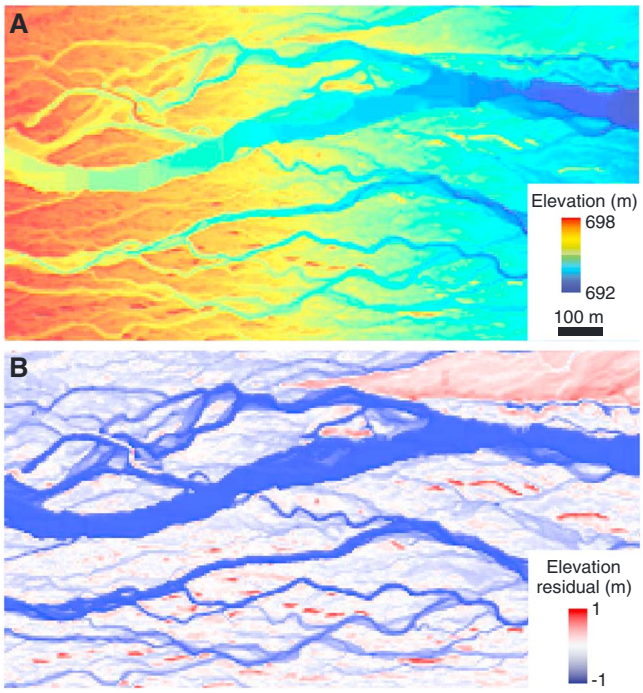

Figure 3. A subset of the DEM for the Platte River. (a) Shaded relief, colorized by elevation. DEM artifacts in the widest channel have been smoothed. (b) Residual elevation after removing a planar trend. Scale and extent are fixed in both panels. Figure 1a shows the full extent of the DEM.

Human activities have dramatically influenced the Platte River in Nebraska. Prior to the 1880s, a braided channel pattern with unvegetated bars prevailed. Major dams constructed in the early twentieth century reduced discharge downstream: near Overton, NE, and the study reach, Randle and Samad (2003) report a decline in the 1.5 year peak flow from 549 m^3/s (1895 to 1909) to 134 m^3/s (1970 to 1999). The maximum wetted width of the river decreased as much as 90% and woody vegetation colonized the braid plain (Johnson, 1998; US Dept. Interior, 2006). Fotherby (2009) notes that multithread reaches correlate with confinement by topography or built structures (e.g., bridges). Braided channels are most visible at low discharges and are obscured at higher discharges (Smith, 1971). Sand composes the channel bed and bars and is accompanied in the bank materials by fine gravel and loam (Smith, 1971; Williams, 1978).

I demonstrate the analysis using a lidar DEM, which has the same extent as Figure 1a and roughly corresponds to reach 3A of Fotherby (2009). Figure 3a shows a detailed view of the DEM, which shows an eastward valley slope. The lidar data were acquired in 2009 after leaf loss from vegetated areas. The survey used a maximum ground sample distance of 1.4 m, with a corresponding root-mean-square elevation error of 18.5 cm. The topography preserves numerous channels (Figure 3a) that are no longer inundated under the present, highly regulated discharge regime. For example, Fotherby (2009) reported that the observed braiding index does not typically exceed three.

To reduce the influence of high-frequency noise on local slope calculations, a two-dimensional Wiener filter is applied to the DEM (Pelletier, 2004) with a 10 × 10 pixel window. Artifacts in raw DEM are evident for the widest channel, whose bathymetry was not resolved due to light absorption by water (Legleiter, 2013). Other studies have modeled channel bathymetry using optical images (Bertoldi et al., 2011; Fonstad & Marcus, 2005; Javernick, Brasington, & Caruso, 2014; Legleiter, 2012, 2013) and in rare cases water-penetrating lidar (Kinzel, Legleiter, & Nelson, 2013).

This paper tests the utility of data set that does not capture the full channel bathymetry. The analysis that follows relies on modeled inundation extent, which could change in response to topographic artifacts that improperly steer flow. Therefore, I apply a set of image operations summarized here. Artifacts in the raw DEM appear as facets with extremely low curvature unrealistic for natural topography in fluvial landscapes. A curvature threshold ($\nabla^2 z < 2.5 \times 10^{-5}$ m^{-1}) identifies these facets, and objects in this image mask are merged using image filtering and binary image morphologic operations. Elevation values for pixels in the mask are replaced using the minimum elevation in a local neighborhood that excludes masked pixels. This procedure smoothes the topography in areas affected by artifacts. To balance model run time with the ability to resolve major bar and channel structure, the DEM grid spacing was then downsampled from 2 m to 10 m.

Previous studies have noted cases in which channels can be mapped using local topographic statistics including curvature and relief (Fagherazzi et al., 1999; McKean et al., 2009; Pirotti & Tarolli, 2010). While informative, neither statistic is sufficient to capture channel paths for the Platte River. For example, Figure 3b shows the DEM after removing the eastward dipping regional slope of 0.001. The resulting map shows bars and channels as relative lows and bars as relative highs. Notably, the area includes channels with a range of widths from near the DEM grid spacing to several tens of pixels wide. This range of channel widths complicates the curvature-based approach, for which the spatial window of the curvature calculation should scale with feature of interest (Pirotti & Tarolli, 2010). Moreover, for the narrower channels, the local elevation residual is less distinct from the background and areas of relatively low elevation can be discontinuous. Therefore, local relief in the detrended DEM does not clearly define the full channel network. The next section turns to channel extraction based on flow modeling.

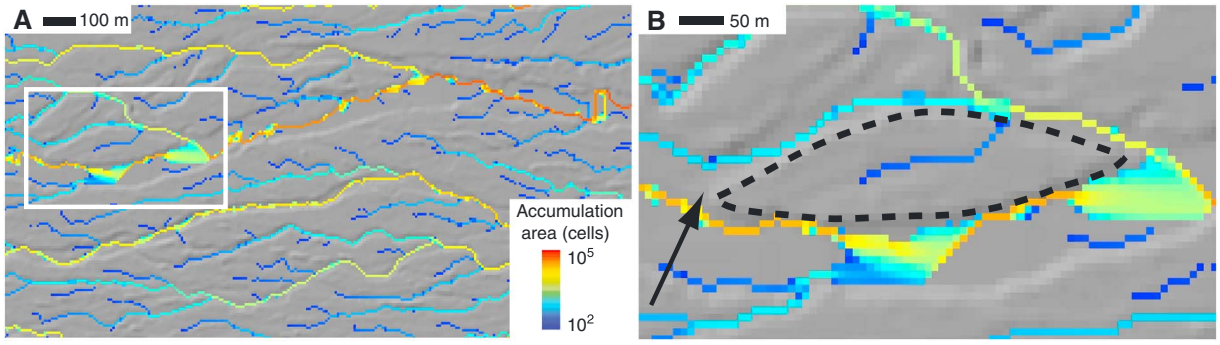

Figure 4. Modeled channel paths colored by drainage area, calculated using Terraflow (Arge et al., 2003), which includes a multiple flow direction algorithm similar to that by Freeman (1991). In both panels, the shaded relief of topography is overlain by accumulation area with a threshold of 100 cells, and the color scale is the same. (a) Overview with extent equivalent to Figures 5a and 5b. The white box indicates the extent of the (b) detailed view. In Figure 4b, the black dashed line is the manually mapped boundary of a bar. The black arrow indicates the upstream edge of the bar, which is not delineated by the algorithm.

3. Channel Extraction and Morphometry

This section describes flow modeling results for the Terraflow and LISFLOOD-FP algorithms and then methods for channel and bar network extraction using modeled inundation. The Terraflow algorithm introduces a unit, fictitious flow at each cell in the DEM and routes it through other cells according to local surface slopes (Figure 2a). Figure 4a shows the resulting map of contributing area for the section of the Platte River DEM in Figure 3a, with areas of relatively high and low contributing area. Intersecting threads of relatively high contributing area bound areas with relatively low contributing area, thus mimicking the underlying patterns of channels and bars, respectively. The connected threads of relatively high contributing area highlight narrow channels with widths similar to the DEM grid spacing. The limitations of the algorithm for channels wider than the grid spacing—namely, that width is not resolved and channel paths are irregular—are consistent with previous results for type 1 channel networks. Yet overall, the Terraflow algorithm captures aspects of the channel network, and at relatively low computational cost compared to a depth-resolving model.

A more unexpected result of the flow routing algorithm is that it fails to consistently capture a key feature of the channel network: flow bifurcation around islands. Figures 4a and 4b show numerous channel threads that are only connected to the channel network at confluences, causing the appearance of isolated channel heads. Although flow can diverge at the scale of a grid cell (Figure 2a), the algorithm still preferentially routes flow down steeper slopes (equation (1)) and importantly does not route flow over adverse slopes if a positive downhill slope borders the contributing cell. In the case of a channel bifurcation, this behavior implies that at a bifurcation that splits a single channel into two, if one of the channel threads has a slightly higher bed elevation, the flow routing algorithm may route flow only down the lower channel thread.

This limitation of mapping using a flow routing algorithm based on land surface slopes alone motivates using a model that also accounts for the water surface. In contrast to a precipitation source, which is implicit in the Terraflow model, the LISFLOOD-FP model can also represent flow for a point source. The way that flow enters the domain influences flow model results, and for flow to serve as a mapping tool, it must interact with the area of interest in the DEM. A localized source is convenient for introducing flow to a channel, and I modify this approach to enable supply to multiple channels at the inlet. In a typical CAESAR-LISFLOOD model run, flow expands from the point source according to the discharge and the local topography. To ensure that flow interacts with channels across the full braid plain, however, the point source is placed in a synthetic reservoir appended to the upstream (west) edge of the domain. The reservoir width is set slightly larger than the width of the braid plain. Flow emanates from a point source placed within the reservoir, which it gradually fills. Walls of arbitrary height, and with elevation greater than the maximum DEM elevation, are placed on the edges of the reservoir that do not coincide with the edge of the original DEM. Thus, flow eventually overtops the reservoir and moves onto the DEM. The reservoir length (perpendicular to the braid plain) is arbitrary and is set to be sufficiently large to moderate transient differences in water surface elevation between the reservoir and the nearest edge of the DEM.

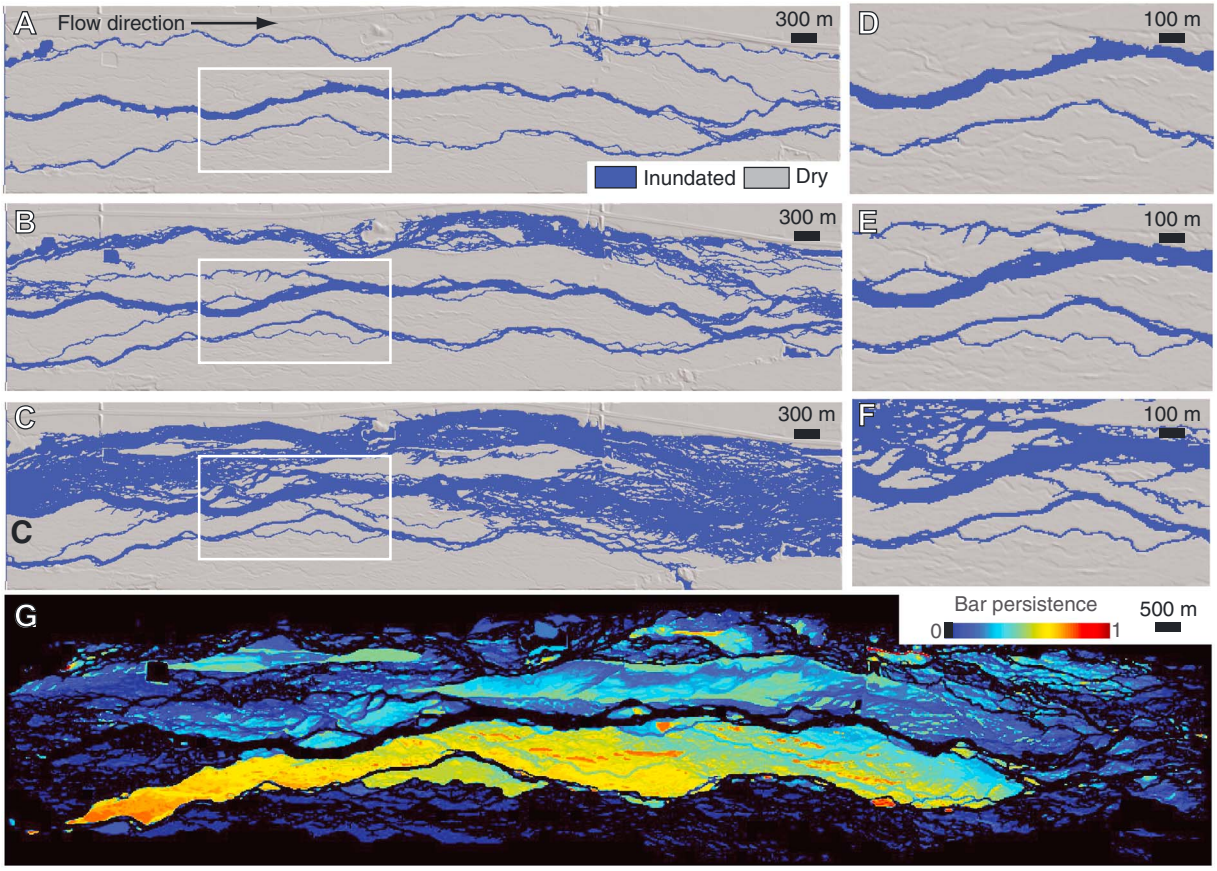

Figure 5. (a–c) Shaded relief maps of the Platte River valley overlain by inundated extent (blue) calculated with the LISFLOOD-FP model for different values of the dimensionless discharge (Q^*). Flow direction is from left to right. (a) $Q^* = 0.18$. (b) $Q^* = 1.40$. (c) $Q^* = 7.03$. The white boxes in Figures 5a–5c indicate the locations of detailed views in Figures 5d–5f, respectively. Scale and extent are constant for Figures 5a–5c and Figures 5d–5f. (g) Bar persistence, measured as the fraction of modeled discharges for which each bar surface remains dry.

In contrast to algorithms based on cell contributing areas (e.g., Freeman, 1991), the CAESAR-LISFLOOD model can be applied for different discharges. The model routes flow until it reaches the DEM boundary. Differences between the discharge entering and leaving the domain can occur initially due to storage in local topographic minima and the time required for flow propagation. These differences decay as the model run proceeds. Therefore, the input discharge is held steady until the disparity between input and output discharge falls below 5%, achieved for this case with a 1 h duration for each discharge (Table 1). Flow depth throughout the model domain is recorded before proceeding to a new model discharge. The model results span 20 logarithmically spaced discharges from 10 to 1000 m^3/s that progress from minimal to extensive inundation of the braid plain. Discharge (Q) can be recast in dimensionless form using a single length scale: commonly, the median grain size (e.g., Parker et al., 2007). Here the chosen dimensionless form is

$$Q^* = \frac{Q}{g^{1/2} L_z^{5/2}} \tag{6}$$

where L_z is a representative length scale, chosen as the standard deviation of elevation in the residual DEM (Figure 3b). Unlike grain size, this length scale can be measured from the topography. Dimensionless discharge (Q^*) varies from 0.14 to 14.0.

Figure 5 shows images of inundated extent for three discharge levels. The planform geometry and extent of bars change for each discharge. For $Q^* = 0.18$ (Figure 5a), the flow introduced across the width of the braid plain concentrates in a subset of channels a subset of the channels including the widest channel. Flow separates around bars at a range of scales, with the largest bars extending several kilometers downstream. In contrast to the Terraflow results, the CAESAR-LISFLOOD model causes flow to spread out across the full width of the wetted channels. This behavior occurs for channels with widths both similar to and significantly larger

than the DEM grid cell width. Flow paths are spatially continuous, and they diverge and converge smoothly around bars and islands resolved by the DEM. In general, both channel threads downstream of each bifurcation are inundated. Driving flow using the water surface rather than the topographic surface reduces flow path sensitivity to artifacts in the DEM.

Figure 5b shows a second model example with $Q^* = 1.40$. The higher modeled discharge compared to Figure 5a causes flow to enter more channel threads and thus reveal additional bar and channel structure, including the structure of smaller bars within larger bars. Bar scale decreases in places as the large bars are dissected by channels activated by the higher discharge. The spatial extent of bars also changes as the higher discharge inundates a broader section of the braid plain. A further increase in modeled discharge to $Q^* = 7.03$ (Figure 5c) causes similar changes in bar and channel geometry mapped by flow. A wide zone of inundation spans much of the domain and surrounds bars of disparate scales. Detailed views of these three discharges (Figures 5d–5f, respectively) show step changes in the detailed structure of bars and channels with increasing discharge. In contrast to the model results in Figure 4b that do not account for the water surface, Figures 5e and 5f show bars as clearly defined by the inundated areas.

These three examples show that increasing modeled discharge causes the flow to define new bars, while also causing other bar surfaces to disappear beneath the water surface. Bar exposure persists through increasing discharge to varying degrees. Figure 5g quantifies this bar persistence as the fraction of modeled discharges for which each pixel remains dry, excluding pixels that were not inundated for the highest discharge. This image shows a large zone of generally high bar persistence extending from upstream to downstream, with internally heterogeneous bar persistence values. This pattern occurs for most of the other bar areas.

In summary, modeling a sequence of escalating discharges gradually reveals the structure of the channel network. In detail, inundation results depend on the chosen flow model and its implementation. Nonetheless, the approach of defining channel and bar features using a flow model can be generally applied. Results from a flow model can clearly distinguish bars and channels (Figures 5e and 5f), and bar surfaces show large spatial heterogeneities in their persistence across the modeled discharge range (Figure 5g). For the analyses that follow, flow depth data from the model run are intermittently recorded to create a binary image of channels, defined as inundated areas, and bars, defined dry areas bounded by inundated areas. Bars and inundated areas are automatically identified for geometric analysis.

4. Bar and Channel Geometry in the Platte River

This section applies the bar and channel extraction technique, using the CAESAR-LISFLOOD flow model, to quantify changes in bar and channel geometry as a function of modeled discharge for the Platte River study site. Importantly, the objective in this case study is not to reproduce specific observations of inundated extent. Several factors would complicate such a comparison, including the simple parameterization of roughness, inaccuracies in the bathymetry, and the high likelihood of topographic change between the acquisition times of image and topography data sets. Instead, this section focuses on the statistics of channel network geometry that are directly accessible from topography data at a fixed time.

4.1. Bar Geometry

Figure 6a shows the number of bars versus dimensionless discharge (equation (6)). Starting from $Q^* = 0.18$, the number of bars varies smoothly as discharge increases. First, the number increases gradually, then more rapidly until it reaches a peak of approximately 1350 bars at $Q^* = 5$, and then declines. Dimensionless bar area (Figure 6b) is more sensitive to dimensionless discharge and increases by more than 1 order of magnitude for a small increase in dimensionless discharge near $Q^* = 0.4$. This dramatic bar area increase occurs because the increase in discharge causes a step change in inundation pattern such that a large new area is bounded by flow and defined as a bar. Subsequent changes in dimensionless bar area with increasing dimensionless discharge are comparatively subtle. Dimensionless bar area increases gradually to a peak near $Q^* = 2$, then declines more rapidly with increasing Q^*.

Figure 6c shows a scatterplot of bar aspect ratio (L_{bar}/w_{bar}) versus dimensionless bar length (L_{bar}/L_z) for the bar populations from each of the three example discharges in Figures 5a–5c. The number of bars and their dimensions vary between these three cases due to the spatial differences in inundation. For all three modeled discharges, bars become more elongate relative to their width as bar scale increases. Least squares

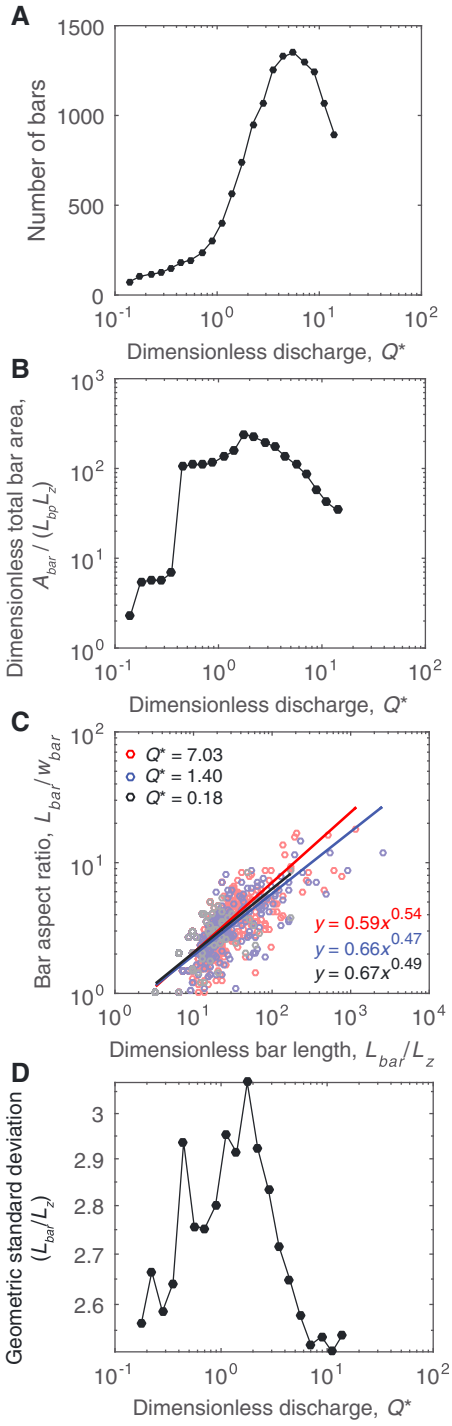

Figure 6. Bar geometry for the Platte River. (a) Number of bars versus dimensionless discharge (Q^*). (b) Total dimensionless bar area versus Q^*. (c) Bar aspect ratio versus dimensionless bar length (L_{bar}/L_z) for the three discharges in Figures 5a–5c. (d) Geometric standard deviation of dimensionless bar length versus Q^*.

fits to each population of bars all show that bar geometry is anisotropic, with bar aspect ratio increasing with dimensionless bar length following an exponent of 0.49 to 0.54.

Figure 6d shows the geometric standard deviation of dimensionless bar length (L_{bar}/L_z), which reflects the variety in scale of the mapped bars, versus dimensionless discharge. In contrast to the number of bars (Figure 6a) and bar area (Figure 6b), the curve in Figure 6c shows more than one local maximum. Nonetheless, there is an overall rise and fall with increasing Q^*, with a peak value near $Q^* = 2$.

In summary, bar planform geometry varies systematically with increasing discharge. For the modeled discharge range, the number of bars (Figure 6a), the total bar area (Figure 6b), and the geometric standard deviation of bar length (Figure 6d) all show maxima at intermediate values of Q^*. Bar dimensions show quantitatively similar anisotropy measures (Figure 6c) for three distinct discharges that span most of the discharge range.

4.2. Channel Planform Geometry

This section turns from the planform geometry of bars to that of channels mapped using inundation. Figure 7a shows braiding index versus downstream distance (normalized by the width of the braid plain) for the three discharges in Figure 5. The braiding index varies with discharge and downstream distance, but with no consistent trend in the former. As for several of the bar metrics (Figure 6), the mean braiding index (Figure 7b) shows lower values at the extremes of dimensionless discharge and the highest mean braiding index for an intermediate dimensionless discharge near $Q^* = 3$. This peak occurs because starting from $Q^* = 0.14$, increases in discharge deliver flow to more channels, which raises the braiding index (Figure 5). Further increases in discharge, however, cause flow to inundate bars. Separate flow threads coalesce into a broader inundated surface, which lowers the braiding index.

The coefficient of variation of braiding index (Figure 7c) does not show a consistent relationship with dimensionless discharge, but instead varies between 0.2 and 0.46. The minimum coefficient of variation of the braiding index occurs near $Q^* = 6$ and is 0.21, which resembles the value of 0.2 reported for experimental braided channels by Egozi and Ashmore (2008) using image analysis.

5. Comparison to Mapping With Flow Depth

In sections 3 and 4, for mapping purposes all wetted areas are treated equally regardless of flow depth. The analysis varies modeled discharge and fixes the threshold depth for distinguishing bars and channels (i.e., depth > 0; Figure 5). This section revisits the bar and channel measures from sections 4.1 and 4.2 using with the complementary approach of fixing the discharge and varying the threshold flow depth. In this sense, the threshold flow depth serves to distinguish deeper channels from shallower channels perched on the braid plain that may activate only at relatively high discharges. To maximize the available range of threshold depths, this analysis uses the model data for the highest discharge ($Q^* = 14.0$). Similarly to the analyses in sections 4.1 and 4.2, the threshold flow depth ($h_{threshold}$) is systematically varied through 20 levels logarithmically spaced between the minimum and the maximum flow depth (h_{max}).

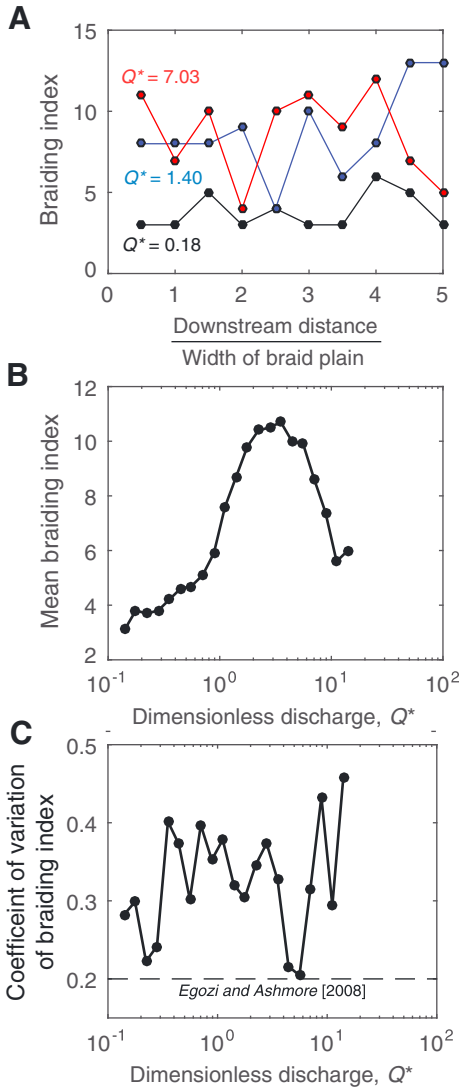

Figure 7. Channel planform geometry for the Platte River. (a) Braiding index versus dimensionless downstream distance for a subset of three dimensionless discharges (Q^*). Braiding index identifies the number of channels and is measured using the number of dry-to-wet transitions in a cross section perpendicular to the mean flow direction. (b) Braiding index versus Q^*. (c) Coefficient of variation of braiding index versus Q^*. The dashed line indicates the coefficient of variation of braiding index for a set of physical experiments by Egozi and Ashmore (2008).

Figures 8a–8c show the mask of areas that meet the flow depth thresholds for three threshold values, each normalized by h_{max}. In each case, $h_{threshold}/h_{max}$ is calibrated to match most closely (within 1%) the areal extent of the inundation-based masks in Figures 5a–5c, respectively. At the scale of the full braid plain (Figures 8a–8c) and in detail (Figures 8d–8f), the channel masks show similarities and differences to their corresponding masks in Figure 5. Lowering the flow depth threshold ($h_{threshold}/h_{max}$) causes the extent of the channel mask to expand from Figure 8a ($h_{threshold}/h_{max}$ = 0.55) to Figure 8b ($h_{threshold}/h_{max}$ = 0.31) and Figure 8c ($h_{threshold}/h_{max}$ = 0.18). This behavior is similar to the increase in channel mask area for increasing modeled discharge in Figures 5a–5c. Despite the equivalent areas of the inundation-based (Figures 5a–5c) and depth-based masks (Figures 8a–8c), for each of the three cases the depth-based mask results in a wider spatial distribution of identified channels. Mapped channels can also appear more abruptly in space, as in Figure 8b, where several mapped channel heads do not connect to a mapped channel upstream. This more discontinuous channel mapping reflects the sensitivity of the depth-threshold map to local changes in topography.

Using the alternate mapping approach of thresholding flow depth, Figure 9 shows the simplest bar and channel statistics for the full set of flow depth thresholds, including the number of bars (Figure 9a), dimensionless total bar area (Figure 9b), and mean braiding index (Figure 9c), versus of the threshold flow depth. All three metrics in Figure 9 peak for intermediate values of dimensionless threshold, similar to the trends obtained with the original mapping approach (Figures 6a–6b and 7c). The dimensionless total bar area (Figure 9b) also reaches a peak value of approximately 10^2, comparable to the result based on varying discharge (Figure 6b). Importantly, however, the peak values in the number of bars (Figure 9a) and the mean braiding index (Figure 9c) are both substantially larger than those obtained from the discharge-threshold approach (Figures 6a and 7c, respectively). In particular, the peak mean braiding index is approximately twice as large using the depth threshold approach (Figure 9c) compared to the discharge-threshold approach (Figure 7c). Compared to thresholding the flow depth map (Figure 8), similar results occurred by thresholding the residual elevation map (Figure 3).

6. Discussion

For the purposes of mapping channels and bars, mapping by inundation while varying modeled discharge represents the simplest approach that realistically reflects spatial patterns of channel activation and bar exposure. The preferred methods proposed here (sections 3 and 4) illuminate the spatial structure of arbitrary channel networks at relatively low computational cost. Several studies have demonstrated the applications of flow models to predicting hydraulics and morphodynamics in multithread rivers (Williams et al., 2016); this paper proposes repurposing inundation models specifically for topographic analysis. The approach successfully captures type 2 channel networks, including multithread rivers, for which previous analyses have been limited in the past by subjectivity in mapping critical elements (Egozi & Ashmore, 2008). Discharge increases affect both sediment transport and the extent of inundation, both of which could alter channel network geometry. The approach here isolates the latter effect. A key distinction from previous studies of channel and bar statistics under observed inundation extents (Egozi & Ashmore, 2008; Marra et al., 2014; Mosley, 1983; Sapozhnikov & Foufoula-Georgiou, 1996) is the ability of the model-based approach to systematically account for changes in the apparent structure of the network due to the extent of inundation.

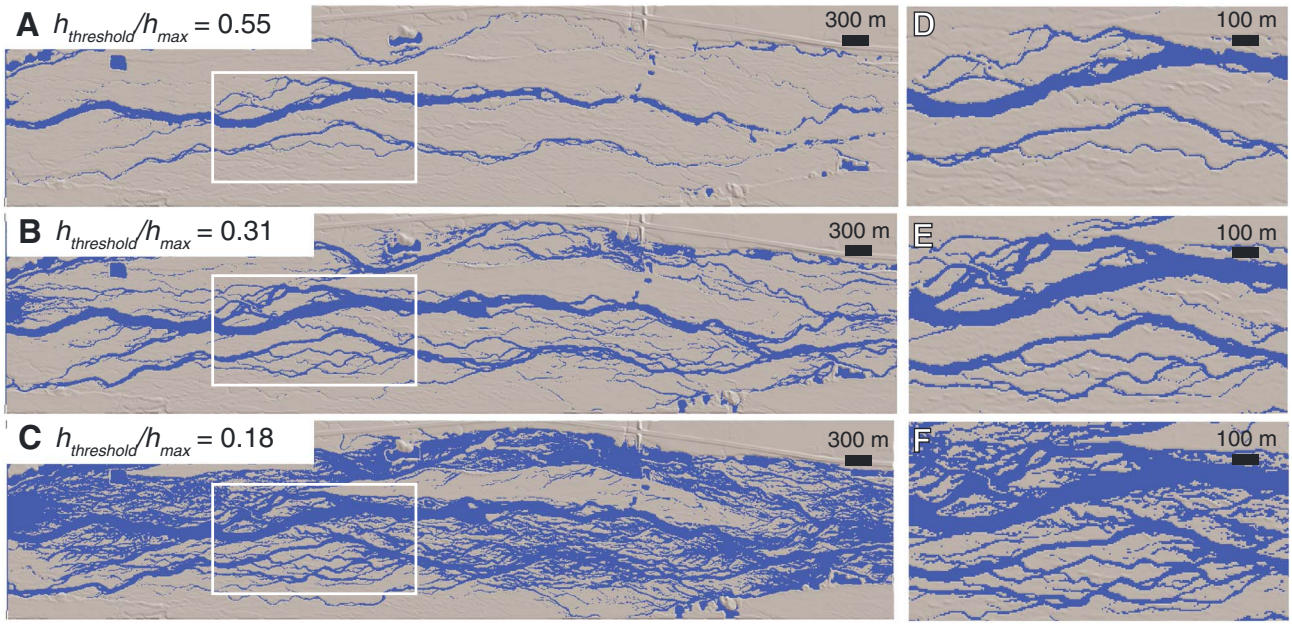

Figure 8. (a–c) Shaded relief maps of the Platte River valley overlain by areas with modeled flow depth greater than $h_{threshold}/h_{max}$ (blue), based on the maximum dimensionless discharge (Q^* = 14.0). (a) $h_{threshold}/h_{max}$ = 0.55. (b) $h_{threshold}/h_{max}$ = 0.31. (c) $h_{threshold}/h_{max}$ = 0.18. The white boxes in Figures 8a–8c indicate the (d–f) locations of detailed views, respectively. Scale and extent are constant for Figures 8a–8c and for Figures 8d–8f.

Mapping using flow introduces two possible approaches based either on fixing the depth threshold and varying the modeled discharge, or vice versa. These approaches can yield similar results for total wetted area (Figures 5 and 8) and bar area (Figures 6b and 8b), and similar overall trends in the number of bars, bar area, and braiding index as a function of the threshold (Figures 6a and 6b and Figure 7 versus Figure 9). Yet the mapping results obtained by either varying the discharge or varying the depth threshold are not equivalent. The depth threshold dramatically over counts the number of channels (Figure 9c versus Figure 7c), and to a lesser extent the number of bars (Figure 9a versus Figure 6a), compared to the discharge-threshold approach. This discrepancy occurs because the depth-threshold approach assumes that all areas that exhibit a similar flow depth for a given discharge will be activated at the same discharge. Instead, to accurately map channels that are active under a particular discharge, explicit modeling of the inundation pattern set by the flow is required.

In contrast to type 1 channel networks, which are successfully extracted using spatial statistics of the land surface alone (Band, 1986; Passalacqua et al., 2010; Tarboton, 1997), a key finding of the present study is that a model that incorporates the water surface is required for accurate extraction of type 2 channel networks from topography data (Figure 5). A flow routing algorithm that allows for multiple flow paths from each DEM grid cell (Figure 2a) is not in itself sufficient to extract the skeleton of a multithread channel network (Figure 4) because it does not permit flow over locally adverse topography if a downslope path is available. Consequently, flow diversions at bifurcations are frequently missed (Figure 4). Algorithms for filling topographic sinks (e.g., Garbrecht & Martz, 1997) that are commonly coupled to flow routing models do not account for this situation in channel networks with divergences. Accounting for the water surface also resolves the wetted width of channels and reduces sensitivity to local slopes the DEM (Figure 5a). To summarize, multiple flow path algorithms do not function like single flow path algorithms for channel network delineation. While neither class of algorithms resolves the channel width, single flow path algorithms do not miss channels where flow paths are convergent. In contrast, multiple flow path algorithms can miss bifurcations and thus miss channel segments. Therefore, multiple flow path algorithms that show diverging flow paths at large scale (Figure 4a; Pelletier, 2004) can yield unrealistically limited flow paths at channel scale (Figure 4b).

In addition to binary images of wetted and dry areas, vector data are useful for calculating statistics for individual bars, channels, and the channel network. The images derived by the flow modeling approach

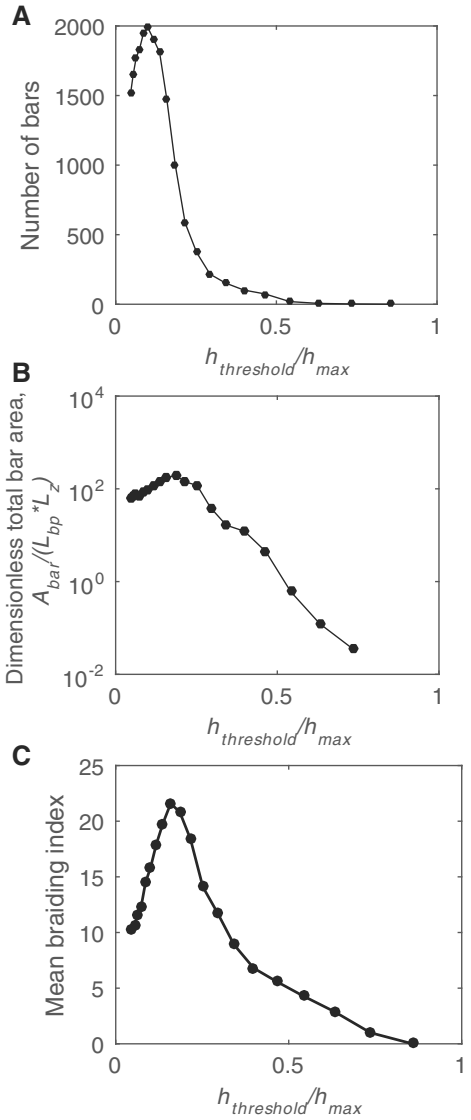

Figure 9. Bar and channel statistics versus threshold flow depth normalized by maximum flow depth ($h_{threshold}/h_{max}$), for then maximum dimensionless discharge ($Q^* = 14.0$). (a) Number of bars versus $h_{threshold}/h_{max}$. (b) Dimensionless total bar area versus $h_{threshold}/h_{max}$. (c) Mean braiding index versus $h_{threshold}/h_{max}$.

(Figure 5) are readily skeletonized to create a vector drainage network of channel centerlines, including the locations of bifurcations and confluences (Marra et al., 2014). A vector channel network encodes a web of spatial relationships between individual channel links that can be further analyzed using techniques from graph theory (De Bartolo et al., 2006; Marra et al., 2014; Tejedor et al., 2015).

To my knowledge, this is the first application of a reduced-complexity flow routing technique expressly to extract the spatial structure of type 2 channel networks. Because of the common use of cellular flow routing procedures in numerical models, this approach is a plausible tool for standardizing comparison between networks generated in numerical models, laboratory experiments, and natural cases. The analysis technique proposed here relies solely on topography and thus complements existing channel mapping techniques that use spectral differences between inundated and dry areas (e.g., Edmonds et al., 2011; Marra et al., 2014).

The Platte River exemplifies the limits of using observed inundation to map channel patterns: many channels are apparent in the topography but are no longer inundated. For such channels, the lack of standing surface water also facilitates acquiring elevation data necessary for flow modeling. The flow modeling approach also opens a way to measure structure for other type 2 channel networks in arid or subaqueous environments, for which observing inundation is impractical. Because of the simplicity of the flow routing scheme, and because the goal is not flow routing per se, this analysis technique is agnostic as to the process for channel formation. This flexibility is advantageous for planetary surface environments where other mechanisms such as lava flow (Dietterich & Cashman, 2014; Leverington, 2004), ice sublimation, debris flows, and mass movements may form and modify channels (e.g., on volcanoes, sediment fans, and gullies along crater rims).

The mapping approach applies only to topographically expressed channels and so cannot reveal channel structure obscured by water or otherwise unresolved by topographic data. Detailed topography data sets are increasingly common for braided rivers (e.g., Bertoldi et al., 2011; Brasington, Vericat, & Rychkov, 2012; Javernick et al., 2014; Thomas & Nicholas, 2002; Wheaton et al., 2010), although the availability of bathymetric data still presents a limitation to widespread application of this method to rivers. Existing techniques for acquiring bathymetry are time-consuming for manual surveys and limited by water depth for bathymetric inversion from remote sensing data (Kinzel et al., 2013; Legleiter, 2013). Yet even with imperfect elevation data (Figure 3a), the analysis demonstrates that several commonly used channel planform statistics including bar dimensions and channel planform statistics can be retrieved.

The new approach differs from channel extraction techniques based on local topographic measures in that it explicitly recognizes the role of the water surface, and the connections it creates, in defining the channel network. The new approach to channel extraction highlights nonlocal spatial relationships and connectivity, including flow paths over adverse topography, which can obscure channels based on topographic measures. In using flow paths to identify channels, the new approach thus complements existing approaches to defining network structure across the spectrum of channel patterns from single-thread, tributary channels in upland landscapes (Passalacqua et al., 2010; Tarboton et al., 1991), to multithread channels in continental interiors, and to deltaic and tidal channels in coastal environments (Edmonds et al., 2011; Fagherazzi et al., 1999; Passalacqua et al., 2013).

Table 2
Summary of Bar and Channel Metrics From Figures 6 and 7

Metric	Dimensionless discharge, Q^*
Number of bars (maximum)	5.59
Dimensionless total bar area (maximum)	1.77
Geometric standard deviation of bar aspect ratio (maximum)	1.40
Mean braiding index (maximum)	3.52
Coefficient of variation of braiding index (minimum)	5.59

The mapping procedure generates inundation maps that are directly comparable to field observations. Using the flow model, discharge variation changes the exposure and number of bars. Bar width and length are anisotropic for all modeled discharges. For three sample discharges, bar aspect ratio increases with increasing bar scale (i.e., bar length increases faster than bar width with increasing scale). Rearranging the fitted scaling relationships between bar aspect ratio and dimensionless bar length from Figure 6c yields $w_{bar} \sim L_{bar}^{0.46–0.53}$. In comparison, Sapozhnikov and Foufoula-Georgiou (1996) also observed anisotropy with bar dimensions measured relative to the overall valley azimuth for braided rivers including the Brahmaputra River, Bangladesh, and the Aichilik and Hulahula Rivers, Alaska. They observed that cross-valley bar dimension (Y) increases more quickly than down-valley bar dimension (X), with $Y \sim X^{1.2–1.3}$ for these cases. The Brahmaputra River data set spanned 2 orders of magnitude in bar scale, similar to the Platte River data set. I speculate that the discrepancy in these scaling relationships between bar width and bar length arises in part from differences valley sinuosity, which changes bar orientation relative to the overall down-valley azimuth (Sapozhnikov & Foufoula-Georgiou, 1996). Vegetation is particularly common in the Platte River study reach and may also influence bar dimensions by stabilizing sediment.

Modeled discharge strongly affects the braiding index, defined as the number of distinct wetted zones in a cross section. A maximum in the mean braiding index (Figure 7a) occurs at an intermediate discharge that optimizes channel inundation with minimal flooding between channels. The rising limb of this relationship is broadly consistent with observations for four rivers in New Zealand (Mosley, 1983). The data set in the latter study does not include spatial averaging, which likely contributes to greater scatter in braiding index. Both laboratory experiments and field measurements have shown a peak in braiding index at intermediate discharge (Egozi & Ashmore, 2009; Welber et al., 2012). For the Platte River, the coefficient of variation of the braiding index (Figure 7c) overlaps with the value observed in experiments by Egozi and Ashmore (2008), which importantly did include morphodynamic adjustment. The similarity in channel statistics between their experiments and the Platte River suggests that despite this difference, laboratory and natural multithread rivers may both nonetheless adjust morphology to a dominant discharge.

Because the apparent arrangement of bars and channels changes with modeled discharge, the inundation modeling approach produces multiple spatial structures (Figure 5) instead of the single result from flow routing based on surface gradients alone (Figure 4). Nonetheless, many applications may require a single representative spatial structure. Which one should we use? Several bar and channel metrics from Figures 6 and 7 are summarized in Table 2, including the number of bars, total bar area, the geometric standard deviation of bar aspect ratio, and the mean and coefficient of variation of the braiding index. Positing that these metrics are each in some way optimized for a particular discharge, Table 2 notes the discharge that corresponds to an extremal value of each metric. These values correspond to maxima in all statistics except the coefficient of variation of braiding index, for which the minimum value agrees with the value reported in the physical experiments of Egozi and Ashmore (2008). For the statistics in Table 2, the corresponding dimensionless discharges all fall in the range of 1.40 to 5.59. This range is relatively narrow compared to the overall discharge range modeled here, which spans 2 orders of magnitude. The corresponding dimensioned discharge is 219 m^3/s. For comparison, the historic 1.5 year peak discharge is 39% lower than the reference discharge for the period 1970 to 1999, but 151% higher than the reference discharge for the period 1895 to 1909, before major flow diversion (Randle & Samad, 2003). The dimensionless discharge for the peak braiding index, which is the most commonly used braiding statistic, falls within the range defined by the other statistics (3.52). Therefore, this paper proposes that the spatial pattern of bars and channels that corresponds to the dimensionless discharge that produces the peak braiding index represents a geometric reference map.

Mapping channel threads using inundation entails two end-member cases. At the limit of no inundation, no channels can be observed; at full inundation, flow overtops all bars and there is only one distinct channel. The latter is often defined as the bankfull condition for a braided river (Brice, 1964; Schumm, 1968; Smith, 1971). Yet as noted in general terms by Rust (1977), some discharge lower than bankfull isolates separate channel threads without fully inundating the bars and is arguably more representative of the channel planform geometry. The model results are consistent with this observation and imply a solution to the conundrum of defining the statistical geometry of braided rivers, which is inherently sensitive to stage height: for a given river, the mean braiding index, which measures the number of channels and thus the intensity of braiding, possesses a representative value that is maximized at a specific discharge. In my view, this particular discharge should be taken as a reference discharge for a multithread channel network, distinct from the bankfull discharge. Therefore, using the approach proposed, the vigor of braiding can in principle be compared for different rivers using this representative, maximum value of the mean braiding index. All other summary channel statistics should be extracted from the pattern corresponding to this index as well. A complication in defining the reference arises in the event that there is no unique maximum in the relationship between mean braiding index and modeled discharge. The likelihood of replicating the noninteger value of the mean braiding index likely decreases as the average number of threads and the downstream extent of the sampled channel network increase.

7. Conclusions

For channel networks with flow divergences, simplified flow models that account for the water surface provide a better means of mapping the connectivity of the channel network than purely topographic methods. In contrast to morphometric analyses based on observed inundation, the flow modeling approach can be used to systematically test the sensitivity of channel planform morphology to changes in inundation under fixed topography. For the Platte River, the new approach reveals that (1) the number, area, and spatial distribution of bars exposed above the modeled water surface changes with discharge; (2) bar length and width scale anisotropically, with scaling coefficients that are relatively insensitive to discharge; and (3) braiding index initially increases as channels are inundated, and then decreases with the inundation of local topographic highs between channels. Thresholding flow model results by flow depth rather than inundation does not accurately capture spatial patterns of channel activation. Comparison of bar and channel statistics versus modeled discharge points to a reference discharge, coincident with the maximum morphologic braiding index, that can be used to compare braided rivers across different discharges. The new channel extraction method extends automated and objective analysis of channel planform morphology to the full spectrum of channel patterns in diverse settings including channels on alluvial fans, deltas, and the seafloor; laboratory experiments; and planetary surfaces.

Acknowledgments

I thank Tom Coulthard and two anonymous reviewers for constructive comments. This work was supported by the National Center for Earth-Surface Dynamics 2 Synthesis Postdoctoral Fellowship Program and the St. Anthony Falls Laboratory Industrial Consortium. I acknowledge the Nebraska Department of Natural Resources for access to elevation data. Chris Paola, Efi Foufoula-Georgiou, Jean-Louis Grimaud, David Mohrig, Paola Passalacqua, Alejandro Tejedor, Patricia Wiberg, and Jon Czuba contributed helpful comments. Digital elevation data and flow model files are available through the Digital Repository for the University of Minnesota (http://hdl.handle.net/11299/190675).

References

Anderson, M. P., Aiken, J. S., Webb, E. K., & Mickelson, D. M. (1999). Sedimentology and hydrogeology of two braided stream deposits. *Sedimentary Geology*, *129*(3), 187–199.

Arge, L., Chase, J. S., Halpin, P., Toma, L., Vitter, J. S., Urban, D., & Wickremesinghe, R. (2003). Efficient flow computation on massive grid terrain datasets. *GeoInformatica*, *7*(4), 283–313.

Ashmore, P. (2013). 9.17 Morphology and dynamics of braided rivers. In *Treatise on Geomorphology* (pp. 289–312). San Diego, CA: Elsevier.

Ashmore, P., & Sauks, E. (2006). Prediction of discharge from water surface width in a braided river with implications for at-a-station hydraulic geometry. *Water Resources Research*, *42*, W03406. https://doi.org/10.1029/2005WR003993

Ashmore, P., Bertoldi, W., & Gardner, J. T. (2011). Active width of gravel-bed braided rivers. *Earth Surface Processes and Landforms*, *36*(11), 1510–1521. https://doi.org/10.1002/esp.2182

Ashworth, P. J., Best, J. L., & Jones, M. A. (2007). The relationship between channel avulsion, flow occupancy and aggradation in braided rivers: Insights from an experimental model. *Sedimentology*, *54*(3), 497–513. https://doi.org/10.1111/j.1365-3091.2006.00845.x

Band, L. E. (1986). Topographic partition of watersheds with digital elevation models. *Water Resources Research*, *22*(1), 15–24. https://doi.org/10.1029/WR022i001p00015

Bates, P. D., Horritt, M. S., & Fewtrell, T. J. (2010). A simple inertial formulation of the shallow water equations for efficient two-dimensional flood inundation modelling. *Journal of Hydrology*, *387*, 33–45. https://doi.org/10.1016/j.jhydrol.2010.03.027

Bertoldi, W., Ashmore, P., & Tubino, M. (2009). A method for estimating the mean bed load flux in braided rivers. *Geomorphology*, *103*(3), 330–340. https://doi.org/10.1016/j.geomorph.2008.06.014

Bertoldi, W., Gurnell, A. M., & Drake, N. A. (2011). The topographic signature of vegetation development along a braided river: Results of a combined analysis of airborne lidar, color air photographs, and ground measurements. *Water Resources Research*, *47*, W06525. https://doi.org/10.1029/2010WR010319

Blair, T. C., & McPherson, J. G. (1994). Alluvial fans and their natural distinction from rivers based on morphology, hydraulic processes, sedimentary processes, and facies assemblages. *Journal of Sedimentary Research*, *64*(3).

Brasington, J., Vericat, D., & Rychkov, I. (2012). Modeling river bed morphology, roughness, and surface sedimentology using high resolution terrestrial laser scanning. *Water Resources Research*, *48*, W11519. https://doi.org/10.1029/2012WR012223

Braun, J., & Sambridge, M. (1997). Modelling landscape evolution on geological time scales: A new method based on irregular spatial discretization. *Basin Research*, *9*(1), 27–52. https://doi.org/10.1046/j.1365-2117.1997.00030.x

Brice, J. C. (1964). Channel patterns and terraces of the Loup Rivers in Nebraska, *U.S. Geological Survey Professional Paper 422-D*. Washington, DC: U.S. Govt. Print. Office.

Bridge, J. S., & Lunt, I. A. (2006). Depositional models of braided rivers. In *Braided rivers: Processes, deposits, ecology and management* (Vol. 36, pp. 11–50). Malden, MA: Blackwell Publishing Ltd.

Burr, D. M., Perron, J. T., Lamb, M. P., Irwin, R. P., Collins, G. C., Howard, A. D., … Baker, V. R. (2013). Fluvial features on Titan: Insights from morphology and modeling. *Geological Society of America Bulletin*, *125*(3–4), 299–321.

Cavalli, M., & Marchi, L. (2008). Characterisation of the surface morphology of an alpine alluvial fan using airborne LiDAR. *Natural Hazards and Earth System Sciences*, *8*(2), 323–333.

Cazanacli, D., Paola, C., & Parker, G. (2002). Experimental steep, braided flow: Application to flooding risk on fans. *Journal of Hydraulic Engineering*, *128*(3), 322–330.

Chow, V. T. (1959). *Open channel hydraulics*. New York: McGraw-Hill.

Coulthard, T. J., & Macklin, M. G. (2003). Modeling long-term contamination in river systems from historical metal mining. *Geology*, *31*(5), 451–454.

Coulthard, T. J., Hicks, D. M., & Van De Wiel, M. J. (2007). Cellular modelling of river catchments and reaches: Advantages, limitations and prospects. *Geomorphology*, *90*(3–4), 192–207. https://doi.org/10.1016/j.geomorph.2006.10.030

Coulthard, T. J., Neal, J. C., Bates, P. D., Ramirez, J., de Almeida, G. A. M., & Hancock, G. R. (2013). Integrating the LISFLOOD-FP 2D hydrodynamic model with the CAESAR model: Implications for modelling landscape evolution. *Earth Surface Processes and Landforms*, *38*(15), 1897–1906. https://doi.org/10.1002/esp.3478

De Bartolo, S. G., Primavera, L., Gaudio, R., D'Ippolito, A., & Veltri, M. (2006). Fixed-mass multifractal analysis of river networks and braided channels. *Physical Review E*, *74*(2). https://doi.org/10.1103/PhysRevE.74.026101

Dietterich, H. R., & Cashman, K. V. (2014). Channel networks within lava flows: Formation, evolution, and implications for flow behavior. *Journal of Geophysical Research: Earth Surface*, *119*, 1704–1724. https://doi.org/10.1002/2014JF003103

Eaton, B. C., Millar, R. G., & Davidson, S. (2010). Channel patterns: Braided, anabranching, and single-thread. *Geomorphology*, *120*(3–4), 353–364. https://doi.org/10.1016/j.geomorph.2010.04.010

Edmonds, D. A., Paola, C., Hoyal, D. C. J. D., & Sheets, B. A. (2011). Quantitative metrics that describe river deltas and their channel networks. *Journal of Geophysical Research*, *116*, F04022. https://doi.org/10.1029/2010JF001955

Egozi, R., & Ashmore, P. (2008). Defining and measuring braiding intensity. *Earth Surface Processes and Landforms*, *33*(14), 2121–2138. https://doi.org/10.1002/esp.1658

Egozi, R., & Ashmore, P. (2009). Experimental analysis of braided channel pattern response to increased discharge. *Journal of Geophysical Research*, *114*, F02012. https://doi.org/10.1029/2008JF001099

Fagherazzi, S., Bortoluzzi, A., Dietrich, W. E., Adami, A., Lanzoni, S., Marani, M., & Rinaldo, A. (1999). Tidal networks 1. Automatic network extraction and preliminary scaling features from digital terrain maps. *Water Resources Research*, *35*(12), 3891–3904. https://doi.org/10.1029/1999WR900236

Farr, T. G., Rosen, P. A., Caro, E., Crippen, R., Duren, R., Hensley, S., … Alsdorf, D. (2007). The Shuttle Radar Topography Mission. *Reviews of Geophysics*, *45*, RG2004. https://doi.org/10.1029/2005RG000183

Fonstad, M. A., & Marcus, W. A. (2005). Remote sensing of stream depths with hydraulically assisted bathymetry (HAB) models. *Geomorphology*, *72*(1–4), 320–339. https://doi.org/10.1016/j.geomorph.2005.06.005

Fotherby, L. M. (2009). Valley confinement as a factor of braided river pattern for the Platte River. *Geomorphology*, *103*(4), 562–576. https://doi.org/10.1016/j.geomorph.2008.08.001

Frankel, K. L., & Dolan, J. F. (2007). Characterizing arid region alluvial fan surface roughness with airborne laser swath mapping digital topographic data. *Journal of Geophysical Research*, *112*, F02025. https://doi.org/10.1029/2006JF000644

Freeman, T. G. (1991). Calculating catchment area with divergent flow based on a regular grid. *Computational Geosciences*, *17*(3), 413–422.

Garbrecht, J., & Martz, L. W. (1997). The assignment of drainage direction over flat surfaces in raster digital elevation models. *Journal of Hydrology*, *193*(1–4), 204–213.

Germanoski, D., & Schumm, S. A. (1993). Changes in braided river morphology resulting from aggradation and degradation. *Journal of Geology*, *451–466*.

Gleyzer, A., Denisyuk, M., Rimmer, A., & Salingar, Y. (2004). A fast recursive GIS algorithm for computing Strahler stream order in braided and nonbraided networks. *Journal of the American Water Resources Association*, *40*(4), 937–946. https://doi.org/10.1111/j.1752-1688.2004.tb01057.x

Hardy, R. J. (2008). Geomorphology fluid flow modelling: Can fluvial flow only be modelled using a three-dimensional approach? *Geography Compass*, *2*(1), 215–234. https://doi.org/10.1111/j.1749-8198.2007.00084.x

Hesse, R., Klaucke, I., Khodabakhsh, S., Piper, D. J. W., Ryan, W. B. F., & NAMOC Study Group (2001). Sandy submarine braid plains: Potential deep-water reservoirs. *AAPG Bulletin*, *85*(8), 1499–1521.

Holmgren, P. (1994). Multiple flow direction algorithms for runoff modelling in grid based elevation models: An empirical evaluation. *Hydrological Processes*, *8*(4), 327–334.

Howard, A. D., Keetch, M. E., & Vincent, C. L. (1970). Topological and geometric properties of braided streams. *Water Resources Research*, *6*(6), 1674–1688. https://doi.org/10.1029/WR006i006p01674

Hundey, E. J., & Ashmore, P. E. (2009). Length scale of braided river morphology. *Water Resources Research*, *45*, W08409. https://doi.org/10.1029/2008WR007521

Javernick, L., Brasington, J., & Caruso, B. (2014). Modeling the topography of shallow braided rivers using Structure-from-Motion photogrammetry. *Geomorphology*, *213*, 166–182. https://doi.org/10.1016/j.geomorph.2014.01.006

Jerolmack, D. J., & Mohrig, D. (2007). Conditions for branching in depositional rivers. *Geology*, *35*(5), 463–466.

Johnson, W. C. (1998). Adjustment of riparian vegetation to river regulation in the Great Plains, USA. *Wetlands*, *18*(4), 608–618.

Kasprak, A., Wheaton, J. M., Ashmore, P. E., Hensleigh, J. W., & Peirce, S. (2015). The relationship between particle travel distance and channel morphology: Results from physical models of braided rivers. *Journal of Geophysical Research: Earth Surface*, *120*, 55–74. https://doi.org/10.1002/2014JF003310

Kelly, S. (2006). Scaling and hierarchy in braided rivers and their deposits: Examples and implications for reservoir modelling. In G. H. Sambrook Smith, J. L. Best, C. S. Bristow, & G. E. Petts (Eds.), *Braided rivers: Process, deposits, ecology and management* (pp. 75–106). Malden, MA: Blackwell Publishing Ltd.

Kim, W., Sheets, B. A., & Paola, C. (2010). Steering of experimental channels by lateral basin tilting. *Basin Research*, *22*(3), 286–301. https://doi.org/10.1111/j.1365-2117.2009.00419.x

Kinzel, P. J., Legleiter, C. J., & Nelson, J. M. (2013). Mapping river bathymetry with a small footprint green LiDAR: Applications and challenges. *Journal of the American Water Resources Association*, *49*(1), 183–204. https://doi.org/10.1111/jawr.12008

Kleinhans, M. G. (2010). Sorting out river channel patterns. *Progress in Physical Geography*, *34*(3), 287–326. https://doi.org/10.1177/0309133310365300

Komatsu, G., & Baker, V. R. (1996). Channels in the solar system. *Planetary and Space Science*, *44*(8), 801–815. https://doi.org/10.1016/0032-0633(96)00010-4

Lallias-Tacon, S., Liébault, F., & Piégay, H. (2014). Step by step error assessment in braided river sediment budget using airborne LiDAR data. *Geomorphology*, *214*, 307–323. https://doi.org/10.1016/j.geomorph.2014.02.014

Lane, S. N., Westaway, R. M., & Murray Hicks, D. (2003). Estimation of erosion and deposition volumes in a large, gravel-bed, braided river using synoptic remote sensing. *Earth Surface Processes and Landforms*, *28*(3), 249–271. https://doi.org/10.1002/esp.483

Lane, S. N., Widdison, P. E., Thomas, R. E., Ashworth, P. J., Best, J. L., Lunt, I. A., … Simpson, C. J. (2010). Quantification of braided river channel change using archival digital image analysis. *Earth Surface Processes and Landforms*, *35*(8), 971–985. https://doi.org/10.1002/esp.2015

Legleiter, C. J. (2012). Remote measurement of river morphology via fusion of LiDAR topography and spectrally based bathymetry. *Earth Surface Processes and Landforms*, *37*(5), 499–518. https://doi.org/10.1002/esp.2262

Legleiter, C. J. (2013). Mapping river depth from publicly available aerial images. *River Research and Applications*, *29*(6), 760–780. https://doi.org/10.1002/rra.2560

Lehner, B., & Grill, G. (2013). Global river hydrography and network routing: Baseline data and new approaches to study the world's large river systems. *Hydrological Processes*, *27*(15), 2171–2186. https://doi.org/10.1002/hyp.9740

Leopold, L. B., & Wolman, M. G. (1957). *River channel patterns: Braided, meandering, and straight*. Washington, DC: U.S. Govt. Printing Office.

Leopold, L. B., & Wolman, M. G. (1960). River meanders. *Geological Society of America Bulletin*, *71*(6), 769–794. https://doi.org/10.1130/0016-7606(1960)71%5B769:RM%5D2.0.CO;2

Leverington, D. W. (2004). Volcanic rilles, streamlined islands, and the origin of outflow channels on Mars. *Journal of Geophysical Research*, *109*, E10011. https://doi.org/10.1029/2004JE002311

Leverington, D. W. (2011). A volcanic origin for the outflow channels of Mars: Key evidence and major implications. *Geomorphology*, *132*(3–4), 51–75. https://doi.org/10.1016/j.geomorph.2011.05.022

Makaske, B. (2001). Anastomosing rivers: A review of their classification, origin and sedimentary products. *Earth Science Reviews*, *53*(3), 149–196.

Marra, W. A., Kleinhans, M. G., & Addink, E. A. (2014). Network concepts to describe channel importance and change in multichannel systems: Test results for the Jamuna River, Bangladesh. *Earth Surface Processes and Landforms*, *39*(6), 766–778. https://doi.org/10.1002/esp.3482

McKean, J., Nagel, D., Tonina, D., Bailey, P., Wright, C. W., Bohn, C., & Nayegandhi, A. (2009). Remote sensing of channels and riparian zones with a narrow-beam aquatic-terrestrial LIDAR. *Remote Sensing*, *1*(4), 1065–1096. https://doi.org/10.3390/rs1041065

Montgomery, D. R., & Foufoula-Georgiou, E. (1993). Channel network source representation using digital elevation models. *Water Resources Research*, *29*(12), 3925–3934. https://doi.org/10.1029/93WR02463

Moore, I. D., O'Loughlin, E. M., & Burch, G. J. (1988). A contour-based topographic model for hydrological and ecological applications. *Earth Surface Processes and Landforms*, *13*(4), 305–320.

Mosley, M. P. (1982). Analysis of the effect of changing discharge on channel morphology and instream uses in a braided river, Ohau River, New Zealand. *Water Resources Research*, *18*(4), 800–812. https://doi.org/10.1029/WR018i004p00800

Mosley, M. P. (1983). Response of braided rivers to changing discharge. *Journal of Hydrology. New Zealand*, *22*(1), 18–67.

Murray, A. B., & Paola, C. (1994). A cellular model of braided rivers. *Nature*, *371*(6492), 54–57. https://doi.org/10.1038/371054a0

Nanson, G. C. (2013). 9.19 Anabranching and anastomosing rivers. In J. F. Shroder (Ed.), *Treatise on geomorphology* (pp. 330–345). San Diego, CA: Academic Press.

Nanson, G. C., & Knighton, A. D. (1996). Anabranching rivers: Their cause, character and classification. *Earth Surface Processes and Landforms*, *21*, 217–239.

Nicholas, A. P., & Sambrook Smith, G. H. (1999). Numerical simulation of three-dimensional flow hydraulics in a braided channel. *Hydrological Processes*, *13*(6), 913–929. https://doi.org/10.1002/(SICI)1099-1085(19990430)13:6<913::AID-HYP764>3.0.CO;2-N

Nykanen, D. K., Foufoula-Georgiou, E., & Sapozhnikov, V. B. (1998). Study of spatial scaling in braided river patterns using synthetic aperture radar imagery. *Water Resources Research*, *34*(7), 1795–1807. https://doi.org/10.1029/98WR00940

O'Callaghan, J. F., & Mark, D. M. (1984). The extraction of drainage networks from digital elevation data. *Computer Vision Graphics, and Image Processing*, *28*, 323–344.

Paola, C. (1996). Incoherent structure: Turbulence as a metaphor for stream braiding. In *Coherent flow structures in open channels* (pp. 705–723). Somerset, NJ: John Wiley and Sons.

Parker, G. (1976). On the cause and characteristic scales of meandering and braiding in rivers. *Journal of Fluid Mechanics*, *76*(3), 457–480.

Parker, G., Shimizu, Y., Wilkerson, G. V., Eke, E. C., Abad, J. D., Lauer, J. W., … Voller, V. R. (2011). A new framework for modeling the migration of meandering rivers. *Earth Surface Processes and Landforms*, *36*(1), 70–86. https://doi.org/10.1002/esp.2113

Parker, G., Wilcock, P. R., Paola, C., Dietrich, W. E., & Pitlick, J. (2007). Physical basis for quasi-universal relations describing bankfull hydraulic geometry of single-thread gravel bed rivers. *Journal of Geophysical Research*, *112*, F04005. https://doi.org/10.1029/2006JF000549

Passalacqua, P. (2016). The Delta Connectome: A network-based framework for studying connectivity in river deltas. *Geomorphology*. https://doi.org/10.1016/j.geomorph.2016.04.001

Passalacqua, P., Belmont, P., & Foufoula-Georgiou, E. (2012). Automatic geomorphic feature extraction from lidar in flat and engineered landscapes. *Water Resources Research*, *48*, W03528. https://doi.org/10.1029/2011WR010958

Passalacqua, P., Belmont, P., Staley, D. M., Simley, J. D., Arrowsmith, J. R., Bode, C. A., … Wheaton, J. (2015). Analyzing high resolution topography for advancing the understanding of mass and energy transfer through landscapes: A review. *Earth Science Reviews*, *148*, 174–193. https://doi.org/10.1016/j.earscirev.2015.05.012

Passalacqua, P., Do Trung, T., Foufoula-Georgiou, E., Sapiro, G., & Dietrich, W. E. (2010). A geometric framework for channel network extraction from lidar: Nonlinear diffusion and geodesic paths. *Journal of Geophysical Research*, *115*, F01002. https://doi.org/10.1029/2009JF001254

Passalacqua, P., Lanzoni, S., Paola, C., & Rinaldo, A. (2013). Geomorphic signatures of deltaic processes and vegetation: The Ganges-Brahmaputra-Jamuna case study. *Journal of Geophysical Research: Earth Surface*, *118*, 1838–1849. https://doi.org/10.1002/jgrf.20128

Pelletier, J. D. (2004). Persistent drainage migration in a numerical landscape evolution model. *Geophysical Research Letters*, *31*, L20501. https://doi.org/10.1029/2004GL020802

Pirotti, F., & Tarolli, P. (2010). Suitability of LiDAR point density and derived landform curvature maps for channel network extraction. *Hydrological Processes*, *24*(9), 1187–1197. https://doi.org/10.1002/hyp.7582

Quinn, P., Beven, K., Chevallier, P., & Planchon, O. (1991). The prediction of hillslope flow paths for distributed hydrological modelling using digital terrain models. *Hydrological Processes*, *5*(1), 59–79. https://doi.org/10.1002/hyp.3360050106

Randle, T. J., & Samad, M. A. (2003). Platte River flow and sediment transport between North Platte and Grand Island, Nebraska (1895-1999), *U.S. Department of the Interior Bureau of Reclamation*. (60 pp).

Redolfi, M., Tubino, M., Bertoldi, W., & Brasington, J. (2016). Analysis of reach-scale elevation distribution in braided rivers: Definition of a new morphologic indicator and estimation of mean quantities. *Water Resources Research*, *52*, 5951–5970. https://doi.org/10.1002/2015WR017918

Reinfelds, I., & Nanson, G. (1993). Formation of braided river floodplains, Waimakariri River, New Zealand. *Sedimentology*, *40*(6), 1113–1127.

Rust, B. R. (1977). A classification of alluvial channel systems. *Fluvial Sedimentology*, *5*, 187–198.

Sangireddy, H., Stark, C. P., Kladzyk, A., & Passalacqua, P. (2016). GeoNet: An open source software for the automatic and objective extraction of channel heads, channel network, and channel morphology from high resolution topography data. *Environmental Modelling and Software*, *83*, 58–73. https://doi.org/10.1016/j.envsoft.2016.04.026

Sapozhnikov, V., & Foufoula-Georgiou, E. (1996). Self-affinity in braided rivers. *Water Resources Research*, *32*(5), 1429–1439. https://doi.org/10.1029/96WR00490

Sapozhnikov, V. B., & Foufoula-Georgiou, E. (1997). Experimental evidence of dynamic scaling and indications of self-organized criticality in braided rivers. *Water Resources Research*, *33*(8), 1983–1991. https://doi.org/10.1029/97WR01233

Sapozhnikov, V., Murray, A. B., Paola, C., & Foufoula-Georgiou, E. (1998). Validation of braided-stream models: Spatial state-space plots, self-affine scaling, and island shapes. *Water Resources Research*, *34*, 2353–2364. https://doi.org/10.1029/98WR01697

Schumm, S. A. (1968). Speculations concerning paleohydrologic controls of terrestrial sedimentation. *Geological Society of America Bulletin*, *79*(11), 1573–1588. https://doi.org/10.1130/0016-7606(1968)79[1573:SCPCOT]2.0.CO;2

Segura, C., & Pitlick, J. (2015). Coupling fluvial-hydraulic models to predict gravel transport in spatially variable flows. *Journal of Geophysical Research: Earth Surface*, *120*, 834–855. https://doi.org/10.1002/2014JF003302

Shelef, E., & Hilley, G. E. (2013). Impact of flow routing on catchment area calculations, slope estimates, and numerical simulations of landscape development. *Journal of Geophysical Research: Earth Surface*, *118*, 2105–2123. https://doi.org/10.1002/jgrf.20127

Smith, N. D. (1971). Transverse bars and braiding in the lower Platte River, Nebraska. *Geological Society of America Bulletin*, *82*(12), 3407–3420. https://doi.org/10.1130/0016-7606(1971)82[3407:TBABIT]2.0.CO;2

Smith, L. C., Isacks, B. L., Bloom, A. L., & Murray, A. B. (1996). Estimation of discharge from three braided rivers using synthetic aperture radar satellite imagery: Potential application to ungaged basins. *Water Resources Research*, *32*(7), 2021–2034. https://doi.org/10.1029/96WR00752

Staley, D. M., Wasklewicz, T. A., & Blaszczynski, J. S. (2006). Surficial patterns of debris flow deposition on alluvial fans in Death Valley, CA using airborne laser swath mapping data. *Geomorphology*, *74*(1–4), 152–163. https://doi.org/10.1016/j.geomorph.2005.07.014

Tal, M., & Paola, C. (2010). Effects of vegetation on channel morphodynamics: Results and insights from laboratory experiments. *Earth Surface Processes and Landforms*, *35*(9), 1014–1028. https://doi.org/10.1002/esp.1908

Tarboton, D. G. (1997). A new method for the determination of flow directions and upslope areas in grid digital elevation models. *Water Resources Research*, *33*(2), 309–319. https://doi.org/10.1029/96WR03137

Tarboton, D., Bras, R. L., & Rodriguez-Iturbe, I. (1991). On the extraction of channel networks from digital elevation data. *Hydrological Processes*, *5*, 81–100.

Tejedor, A., Longjas, A., Zaliapin, I., & Foufoula-Georgiou, E. (2015). Delta channel networks: 2. Metrics of topologic and dynamic complexity for delta comparison, physical inference, and vulnerability assessment. *Water Resources Research*, *51*, 4019–4045. https://doi.org/10.1002/2014WR016604

Thomas, R., & Nicholas, A. P. (2002). Simulation of braided river flow using a new cellular routing scheme. *Geomorphology*, *43*(3), 179–195.

Thomas, R., Nicholas, A. P., & Quine, T. A. (2007). Cellular modelling as a tool for interpreting historic braided river evolution. *Geomorphology*, *90*(3–4), 302–317. https://doi.org/10.1016/j.geomorph.2006.10.025

Tockner, K., Paetzold, A., Karaus, U., Claret, C., & Zettel, J. (2009). Ecology of braided rivers. In G. H. Sambrook Smith, J. L. Best, C. S. Bristow, & G. E. Petts (Eds.), *Braided rivers: Process, deposits, ecology and management* (pp. 339–359). Oxford, UK: Blackwell Publishing Ltd.

Trevena, A. S., & Picard, M. D. (1978). Morphometric comparison of braided Martian channels and some braided terrestrial features. *Icarus*, *35*(3), 385–394.

Tucker, G. E., & Hancock, G. R. (2010). Modelling landscape evolution. *Earth Surface Processes and Landforms*, *35*(1), 28–50. https://doi.org/10.1002/esp.1952

US Dept. Interior (2006). Platte River Recovery Implementation Program final environmental impact statement. Denver, CO: Platte River EIS Office.

Van Der Nat, D., Tockner, K., Edwards, P. J., Ward, J. V., & Gurnell, A. M. (2003). Habitat change in braided flood plains (Tagliamento, NE-Italy). *Freshwater Biology*, *48*(10), 1799–1812.

Volker, H. X., Wasklewicz, T. A., & Ellis, M. A. (2007). A topographic fingerprint to distinguish alluvial fan formative processes. *Geomorphology*, *88*(1–2), 34–45. https://doi.org/10.1016/j.geomorph.2006.10.008

Welber, M., Bertoldi, W., & Tubino, M. (2012). The response of braided planform configuration to flow variations, bed reworking and vegetation: The case of the Tagliamento River, Italy. *Earth Surface Processes and Landforms*, *37*(5), 572–582. https://doi.org/10.1002/esp.3196

Wheaton, J. M., Brasington, J., Darby, S. E., & Sear, D. A. (2010). Accounting for uncertainty in DEMs from repeat topographic surveys: Improved sediment budgets. *Earth Surface Processes and Landforms*, *35*(2), 136–156. https://doi.org/10.1002/esp.1886

Wickert, A. D., Martin, J. M., Tal, M., Kim, W., Sheets, B., & Paola, C. (2013). River channel lateral mobility: Metrics, time scales, and controls. *Journal of Geophysical Research: Earth Surface*, *118*, 396–412. https://doi.org/10.1029/2012JF002386

Williams, G. (1978). The case of the shrinking channels—The North Platte and Platte Rivers in Nebraska, (Vol. 781, pp. 48). Arlington, VA: U.S. Geological Survey Circular.

Williams, G. P. (1986). River meanders and channel size. *Journal of Hydrology*, *88*(1–2), 147–164. https://doi.org/10.1016/0022-1694(86)90202-7

Williams, R. D., Brasington, J., & Hicks, D. M. (2016). Numerical modelling of braided river morphodynamics: Review and future challenges. *Geography Compass*, *10*(3), 102–127. https://doi.org/10.1111/gec3.12260

Williams, R. D., Brasington, J., Hicks, M., Measures, R., Rennie, C. D., & Vericat, D. (2013). Hydraulic validation of two-dimensional simulations of braided river flow with spatially continuous aDcp data. *Water Resources Research*, *49*, 5183–5205. https://doi.org/10.1002/wrcr.20391

Williams, R. M. E., & Malin, M. C. (2008). Sub-kilometer fans in Mojave Crater, Mars. *Icarus*, *198*(2), 365–383. https://doi.org/10.1016/j.icarus.2008.07.013